06

# Carbon framework nanomaterials for stimulation of neural tissue cells

© D.T. Murashko,[1] U.E. Kurilova,[1,2] I.A. Suetina,[3] L.I. Russu,[3] A.V. Kuksin,[1] M.V. Mezentseva,[3] E.P. Kitsyuk,[4] A.G. Markov,[2] D.V. Telyshev,[1,2] A.Yu. Gerasimenko[1,2]

[1] Institute of Biomedical Systems, National Research University of Electronic Technology „MIET“,
124498 Moscow, Zelenograd, Russian Federation
[2] Institute for Bionic Technologies and Engineering, Sechenov First Moscow State Medical University, Sechenov University,
119991 Moscow, Russia
[3] National Research Center for Epidemiology and Microbiology Named after the Honorary Academician N.F. Gamaleya,
123098 Moscow, Russia
[4] Scientific-Manufacturing Complex „Technological Centre“,
124498 Moscow, Russia
e-mail: gerasimenko@bms.zone

*Received November 1, 2024 Revised November 1, 2024*
*Accepted November 1, 2024.*

The paper presents a technology for the formation of carbon framework nanomaterials for the creation of neurointerfaces between electronic stimulating devices and neural tissue cells. Nanomaterials were formed by spray deposition and laser patterning of layers of single-walled carbon nanotubes and reduced graphene oxide. Radiation of the first harmonic of a nanosecond ytterbium fiber laser with a wavelength of 1064 nm and power of 0.07 W provided the formation of an electrically conductive framework of nanotubes, reduced graphene oxide and their hybrid structures, which was demonstrated by scanning electron microscopy and Raman spectroscopy. It is shown that laser exposure provided an increase in electrical conductivity from 1.2 to 3.5 times (up to $37.8 \pm 1.2$ mS for hybrid structures from single-walled carbon nanotubes and reduced graphene oxide). The specified topologies from carbon frame nanomaterials were formed for their use as neurointerfaces with the generator of electrical pulses on the basis of a tablet for cell cultivation. Electrical stimulation in the process of cultivation provides an increase in the number of cells. An increase in the number of cells by 4.3 times for fibroblasts and 2.9 times for neural tissue cells grown on carbon frame nanomaterials compared to cells grown under conventional conditions was obtained. Formed carbon frame nanomaterials are promising for transmission of electrical signals in cell culture devices and other implantable devices, including neurointerfaces.

**Keywords:** carbon nanotubes, reduced graphene oxide, bioelectronics, neural interfaces, electrical stimulation.

DOI: 10.61011/TP.2025.02.60838.368-24

## Introduction

Bioelectronics is currently a rapidly growing field of science. The principle of operation of bioelectronic devices is often associated with electrical signal transmission to biological tissues from electronic circuits via interfaces with various macro-, micro- and nanolevel topologies. Bioelectronic device interfaces interacting with biological tissues shall have high biocompatibility and transmit electronic pulses with as high resolution and signal-to-noise ratio as possible. Bioelectronic devices interfaced with electrically conducting cells such as neurons or cardiomyocytes can record and/or facilitate bioelectrical activity in cells or corresponding tissues (for example, brain, hart or muscles) by means of mutual transformation of ionic and electronic currents at the device–cell interface. Bioelectronic interfaces for electric stimulation of cell adhesion, alignment, proliferation and differentiation that promote regeneration of damaged tissues such as skin, bones, nerves, myocardium tissues, etc., are of particular interest in this case.

Due to combination of their physical and biological properties, carbon nanomaterials are promising materials for creating bioelectronic interfaces stimulating cell growth. Carbon nanotubes and graphene are able to show high mechanical strength and stability due to $sp^2$-hybridized structure with high aspect ratio of dimensions which affects the flexibility of extended structures. Carbon nanomaterials have high thermal and electric conductivity and their dimensions and structure are comparable with those of the major extracellular matrix proteins [1]. External impacts by electric field, electronic beam or plasma may be used to create scaffold structures with compounds that are characterized by the$sp^3$-hybridization [2–5]. External impacts result in a nanostructure bending trend, including single-walled carbon nanotubes (SWCNT). Nanotube graphene layer bending leads to formation of defects such as pentagons and heptagon [6]. Pentagonal rings are formed with positive curvature of the graphene layer with the $sp^3$-hybridization, and heptagonal rings are formed with negative curvature of the graphene layer. Due to external impact, controllability of structural, mechanical and electrophysical properties may be achieved.

Carbon nanotubes are often used for creating devices for field potential detection and electrical cell simulation due to high mechanical flexibility, high surface area, good charge transfer and electrochemical properties [7]. For these

applications, the fabricated electrodes shall meet a set of requirements, i.e. to be electrically conducting, to have low impedance, high capacity, and to be biocompatible. For electrostimulation, it is important to deliver the charge such that to activate an action potential without affecting cells. Suitability of carbon nanotubes for creating bioelectronic components used for electrophysiological sensors is reported [8]. For such purposes, a particular sensitivity level shall be ensured when measuring biosignals to facilitate more accurate diagnosis of diseases. Therefore, it is important to ensure close contact between the bioelectronic interface and biological tissue by means of structural compatibility of both sides.

Graphene can be also used to create bioelectronic components because this two-dimensional material has high electron mobility with high surface area [9]. Graphene provides a sensitivity level of bioelectronic components for measurement of electrophysiological human properties in long-term monitoring [10]. Laser irradiation can improve mechanical and electrically conductive properties of carbon nanotubes and graphene oxide. For example, nanosecond laser exposure can create electrically conductive networks from single-walled carbon nanotubes [11] to improve mechanical and electrical properties of samples. Possibility of creating electrically conductive composite nanostructures based on reduced graphene oxide and bovine serum albumin using femtosecond laser radiation was also reported [12]. Similarly, laser radiation may be used to create electrically conductive composite nanostructures based on carbon nanotubes and reduced graphene oxide [13]. Such devices may be used both for stimulating effect to transmit electric pulses to cells and for reading signals from tissue surfaces.

Electrical stimulation is known to improve cell differentiation and proliferation. Ionic currents and electric potentials within cells affect the function and development of cells and tissues. Violation or alteration of ion gradients or surface charges of cells using an applied electric field can cause changes in cell signal paths and gene expression which leads to positive changes in cell differentiation, proliferation and mobility. Electrical cell stimulation causes accelerated cell growth, improved cell adhesion, augmented interaction between cells and increased cell viability.

This work discusses a carbon scaffold nanomaterial sample fabrication technique using layer spray deposition and laser structuring methods. Structure and electric conductivity investigation results were obtained for nanomaterial layer samples. Electrical cell stimulation was examined on carbon scaffold nanomaterial samples using a developed system on the basis of a culture plate to improve cell growth of connective and nervous tissues.

## 1. Materials and research methods

### 1.1. Formation of carbon scaffold nanomaterials for cell growth stimulation

To form carbon scaffold nanomaterial samples used as interfaces for connective and nervous tissue cell stimulation, *n*-doped 4.5 Ω-cm, (100) oriented 4 inch silicon wafers (Si-Mat, Landsberg am Lech, Germany) cut into $10 \times 5$ mm rectangular plates were used. A catalytic pair of Ti (10 nm) and Ni (2 nm) was deposited onto a substrate treated in Piranha solution by the electron beam vapor deposition method. Then, homogenous dispersed media were formed and contained SWCNT (Universal Additives, Novosibirsk, Russia), reduced graphene oxide (RGO) (Grafenoks, Chernogolovka, Russia) and hybrid SWCNT and RGO structures with component concentrations of 0.1 and $0.05/0.05\,\mu$g/ml, respectively. Dispersed media formation process is shown in Figure 1.

These dispersed media were deposited layer-by-layer on the substrate surfaces by means of spray deposition implemented using the E2V (Nordson EFD, Westlake, OH, USA) dosing system with a 0.5 mm outlet nozzle. Dispersed medium supply pressure was equal to 2 bar. Samples were placed on a heating table to evaporate liquid at 70°C. Up to 50 dispersed medium layers were deposited on each substrate.

### 1.2. Laser formation of the pre-defined topology of carbon scaffold nanomaterials for nervous tissue cell stimulation

To improve electrical conductivity, the deposited coatings were structured by laser radiation exposure. Pre-defined topology layout was also formed to investigate cell distribution on the sample surface. Laser formation of the topology was performed using an ytterbium optical fiber laser with a wavelength of 1064 nm, pulse duration of 100 ns, frequency of 30 kHz and radiation power range of 0.07–0.27 W. The above-mentioned parameters were set using software for a computer connected to the laser system. The system has a galvanometric scanner with two mirrors to move the laser beam. Positioning accuracy was equal to $1.0 \pm 0.2\,\mu$m and radiation focusing was performed using a lens with a focal distance of 210 mm to a diameter of $35\,\mu$m. The spatial profile of linearly polarized radiation had a shape of the Gaussian distribution. To ensure uniform radiation distribution throughout the exposed area, the system includes a proximity sensor.

Laser formation of samples was performed along a software-specified route. For structuring of the samples, a rectangular motion path was defined in software, however, to form samples with the desired topology, the beam path was set as letter „Sh“. Both figures were filled with lines that partly overlapped each other. This was made to partly compensate the intensity of laser radiation with the Gaussian distribution. Beam motion rate along the specified path was 240 mm/s. The length of laser pulse lines was in the range of 5–10 mm, the lines themselves were parallel to each and spaced at $17\,\mu$m between each other. Schematic diagram of the topology formation process is shown in Figure 2.

Thus, the study included the following groups of samples from layers with pre-defined topology on a silicon chip from:

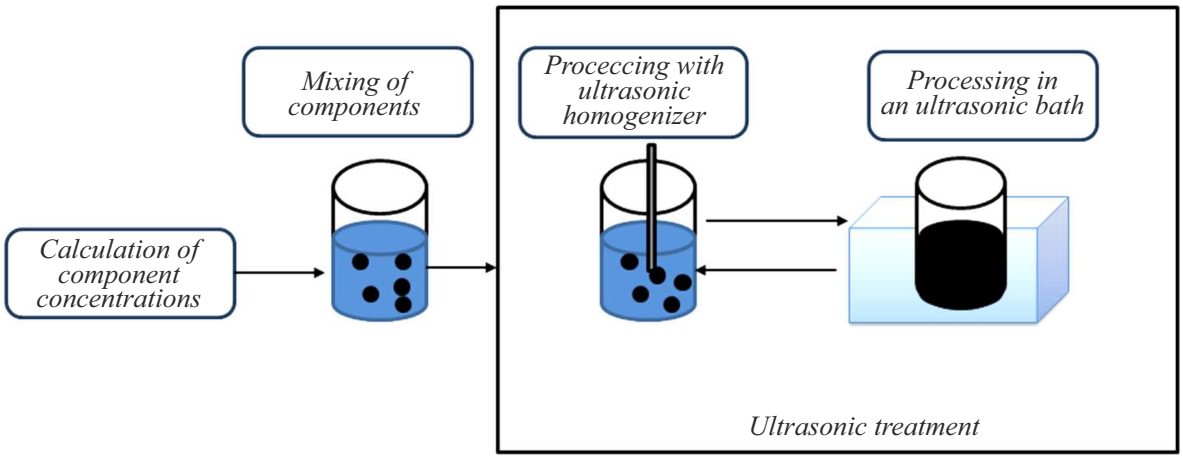


**Figure 1.** Process of formation of dispersed media with carbon nanomaterials.

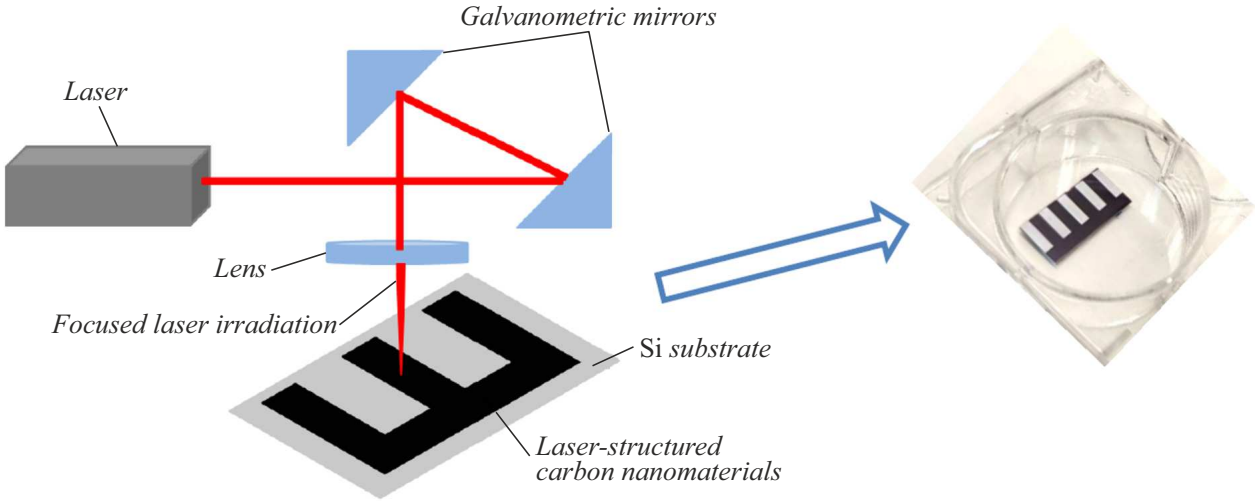


**Figure 2.** Process of sample formation from carbon nanomaterials according to a pre-defined topology.

1) SWCNT; 2) SWCNT structured by laser radiation; 3) RGO; 4) RGO structured by laser radiation; 5) SWCNT and RGO hybrid structures; 6) SWCNT and RGO hybrid structures structured by laser radiation. Four samples were made for each of the represented groups. Pure silicon substrate served as a test sample.

### 1.3. Scanning electron microscopy.

Structural features of the samples on silicon wafers were studied by means of scanning electron microscopy (SEM) using the FEI Helios NanoLab 650 microscope (FEI Ltd., Hillsboro, OR, USA). Accelerating voltage was equal to 5 kV, electronic probe current was equal to 86 pA for samples with SWCNT, RGO and SWCNT+RGO. Vacuum chamber pressure was $7.04 \cdot 10^{-4}$ Pa. Samples were attached to a conducting substrate using carbon adhesive tape.

### 1.4. Raman scattering spectroscopy

Raman scattering spectroscopy is an effective method to detect atomic-level changes in samples. This method, when used in respect of nanocarbon materials, makes it possible to assess the their purity, functionalization features, presence and magnitude of defects. Raman scattering spectra of carbon scaffold nanomaterials for creating neurointerfaces were obtained in back scattering layout using the inVia Qontor spectrometer (Renishaw plc, New Mills, UK). Spectra were measured using a 1200 1/mm grating, a 532 nm semiconductor laser served as an excitation source. Laser beam was focused on the sample surface using a built-in microscope with a $\times 50$ lens. Measurements for each sample were performed in three random points, calibration by measuring pure silicon spectra was performed before measuring a sample surface spectrum.

### 1.5. Electric conductivity measurement

Resistance of the samples was measured by a four-probe measurement method using a measuring system (JG ST-2258C, Jingge Electronics Co., China). A series of resistance measurements was conducted for each of the samples with each value of resistance recalculated into electric conductivity ($\sigma$). After this, the values of electric conductivity were averaged.

### 1.6. Electric stimulation

An experimental system was developed for electric stimulation of cell growth. Sterile acupuncture needles made of gold-flashed surgical steel were used as electrodes. Electrode diameter was 0.3 mm. Such needles are often used in medical applications. Materials used in their manufacturing are highly compatible with biotissues and are capable of transmitting electric current in sufficient amount. Electrode needles were bent at 90° with respect to a breadboard to which they were soldered. Needle tip that adjoined the sample surface was also bent, thus, forming a looped shape. This shape was required to ensure soft non-damaging contact between the sample and electrode. The other electrode end was soldered to the breadboard in such away as to ensure springing in contact with the sample surface. Each culture plate well contained two electrodes (positive and negative) spaced at 24 mm. Two 0.4 mm holes were made in the culture plate cover. Their layout corresponded to the position of electrodes passing through the plate holes. General view of the system is shown in Figure 3.

The electrical stimulation system included a 6-well plate, electrodes, pulse generator, power supply and connecting elements. A „Krona (6F22)“ 9 V zinc-manganese battery was used as power supply. During electrical stimulation, all system components were placed in a $CO_2$ incubator. The incubator provided the required ambient conditions (i.e. 37°C and concentration of $CO_2$ in air equal to 5%) for cell activity.

MTS assay was used to find that optimum pulse generator parameters for electrical stimulation of cell growth are provided be means of continuous sequence of pulses with an amplitude of 80 $\mu$V. Pulse repetition rate was 400 Hz, and pulse duration was 1.2 s [14].

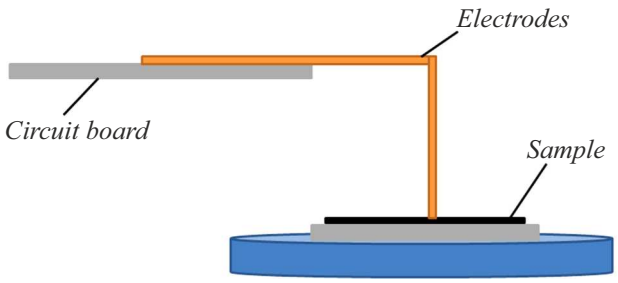


**Figure 3.** Schematic view of the cell growth electrostimulation system.

### 1.7. Cell culture

A fibroblast cell line (FCL) produced by the Gamaleya National Center of Epidemiology and Microbiology was used for the experiments. Cells were grown in Dulbecco's modified Eagle (DMEM) — 90% of culture solution with addition of 10% calf serum in a 6-well plate. The accurate number of cells involved in the experiment was calculated directly before seeding the culture mixture into wells with carbon scaffold nanomaterial samples. To determine an accurate number of cells,an autocellcounter (Scepter Millipore, Merck KGaA, Darmstadt, Germany) was used. FCL cell seed dose was $2 \cdot 10^5$ cells/ml. 2.5 ml of cells were added into each well of the 6-cell plate. Then, cells were incubated in a thermostat during 24 h at 37°C and with CO2 concentration in air equal to 5%.

The study also used the Neuro 2A tissue cells produced by the Gamaleya National Center of Epidemiology and Microbiology — mouse glioblastoma cell line. Cell preparation procedure is similar to FCL cell preparation. The Neuro 2A cell seed dose was $2.7 \cdot 10^5$ cells/ml, 2.5 ml of cells were added into each well.

Cell study samples were prepared in sterile conditions. After fabrication, the samples were irradiated in a bactericidal chamber at ultrasound radiation during 20 min. Directly before the experiment, the samples and electrodes were rinsed in gentamycin culture medium (25 $\mu$l per 50 ml of medium). For this, the samples were placed on the bottom of wells, then the wells with samples were filled solution to a height of several millimeters. The solution was held in wells during several minutes and then removed. At the final step,the wells were filled with the cell solution. Cell were grown on the samples during 24 h without electrical stimulation, then a battery was connected and cell growth was continued during 48 h with stimulation.

### 1.8. Cell visualization

Living cells were stained using 10 $\mu$g/ml of the Hoechst 33342 dye (Life Technologies, New York, New York, USA) for staining cell body and nucleus. Cells with Hoechst 33342 were incubated during 15 min at 37°C. Visualization was performed directly after completion of the cultivation using a fluorescent microscope (Olympus BX43, Olympus Corporation, Tokyo, Japan), laser scanning microscope (Olympus FV3000, Olympus Corporation, Tokyo, Japan) and FV31S-SW Viewer software (Olympus Corporation, Tokyo, Japan). Three images were made in each case. A pure silicon wafer without samples was examined as a test sample.

## 2. Experiment

Structure and electric conductivity of the samples were studied to review the improvement of cell metabolism and functionality before and after the electrical stimulation of cell growth on carbon nanotube and graphene topologies

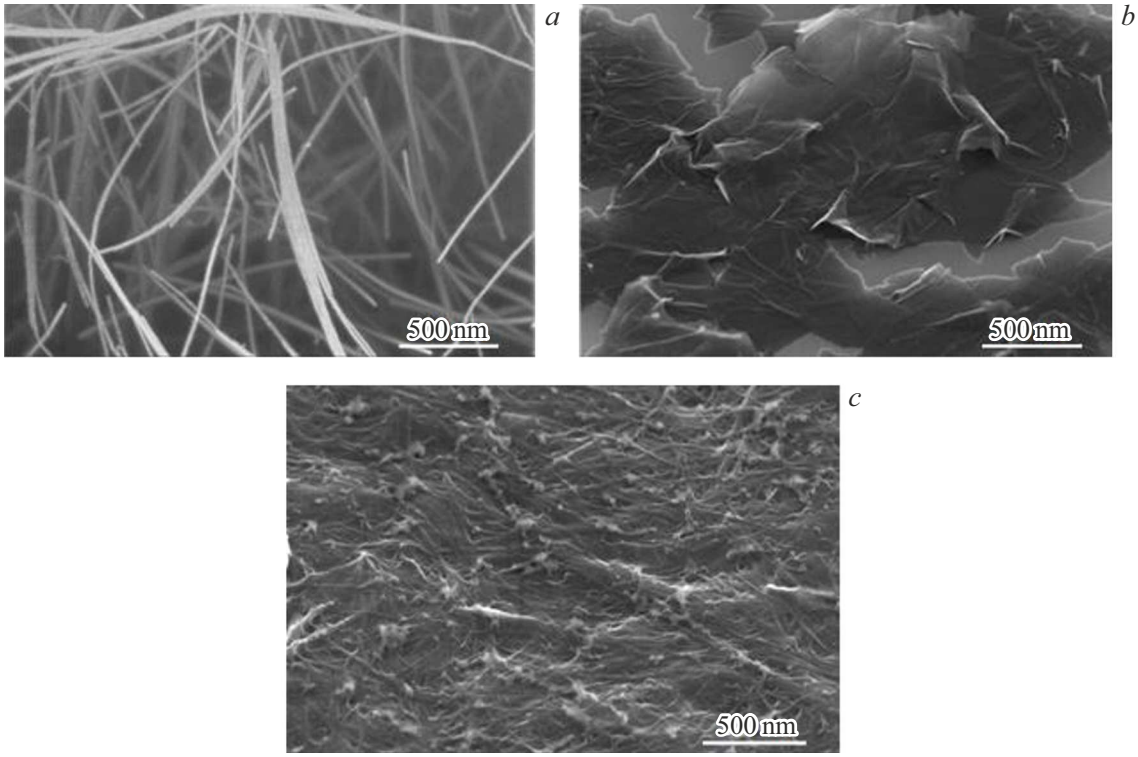


**Figure 4.** Initial view of the samples: *a* — SWCNT, *b* — RGO, *c* — SWCNT and RGO hybrid structures.

before and after laser structuring. The influence of laser structuring and electrical stimulation on cell proliferation was also reviewed.

### 2.1. Morphology of carbon scaffold nanomaterials for nervous tissue cell stimulation

Outside diameter of SWCNT was $1.6 \pm 0.4$ nm, and the length was more than $5\,\mu$m. Figure 4 shows the initial view of the SWCNT, RGO, SWCNT and RGO hybrid structure samples.

These images show that the formed SWCNT sample surface looks like overlapping nanotube bunches irregularly distributed on the substrate surface. These bunches may be observed either as separately standing nanotubes or as interconnected harnesses with a thickness of maximum 2−3 interconnected nanotubes. Outside diameter of one nanotube is $1.6 \pm 0.4$ nm. The presence of layer-by-layer overlapping of the sets of nanotubes, which corresponded to the method used to form the sample (spray deposition method). For the RGO sample, uneven distribution of the RGO particles on the substrate surface thus forming a multilayer coating may be seen. RGO particles themselves had a form of irregular scale leaves with length and widths from 500 to 1000 nm. Images of the SWCNT and RGO hybrid structures showed that the used dispersed SWCNT+RGO medium forms a dense and uniform coating on the substrate surface. The images show numerous overlapping SWCNT layers and RGO particles can be also seen.

Laser radiation is known to facilitate formation of covalent bonds between carbon nanotubes [15]. C−C bonds are formed in most irradiated defective areas of the nanotube scaffold as a result of low thermal conductivity in these areas. As a result, interconnected network areas are formed that improve electric conductivity compared with initial materials on substrates It is also reported that formation of scaffolds is possible under laser radiation as demonstrated in the case of SWCNT based scaffolds in albumin and chitosan biopolymer [16,17]. The structures provided high electric conductivity in biopolymer itself [18,19]. In this case, electric conductivity depends on the morphology of used carbon nanomaterials [20]. Morphology of scaffold materials based on carbon nanotubes and graphene depending on the used laser radiation power was also studied.

To form carbon scaffold nanomaterials for stimulation of nervous tissue cells, a value of power was found experimentally to ensure SWCNT and RGO structuring in nanotube defect areas, as a result a scaffold structure is formed. Structuring was performed under laser radiation with power in the range of 0.07−0.27 W. It was reported that there was no structuring at lower powers. Bonds between SWCNT and RGO are formed under $\geq 0.07$ W laser radiation, radiation energy was absorbed, which causes collision between phonons and carbon atoms and formation of defects in atomic core of nanotubes. Defects are vacant areas and interstices formed due to ballistic collision of

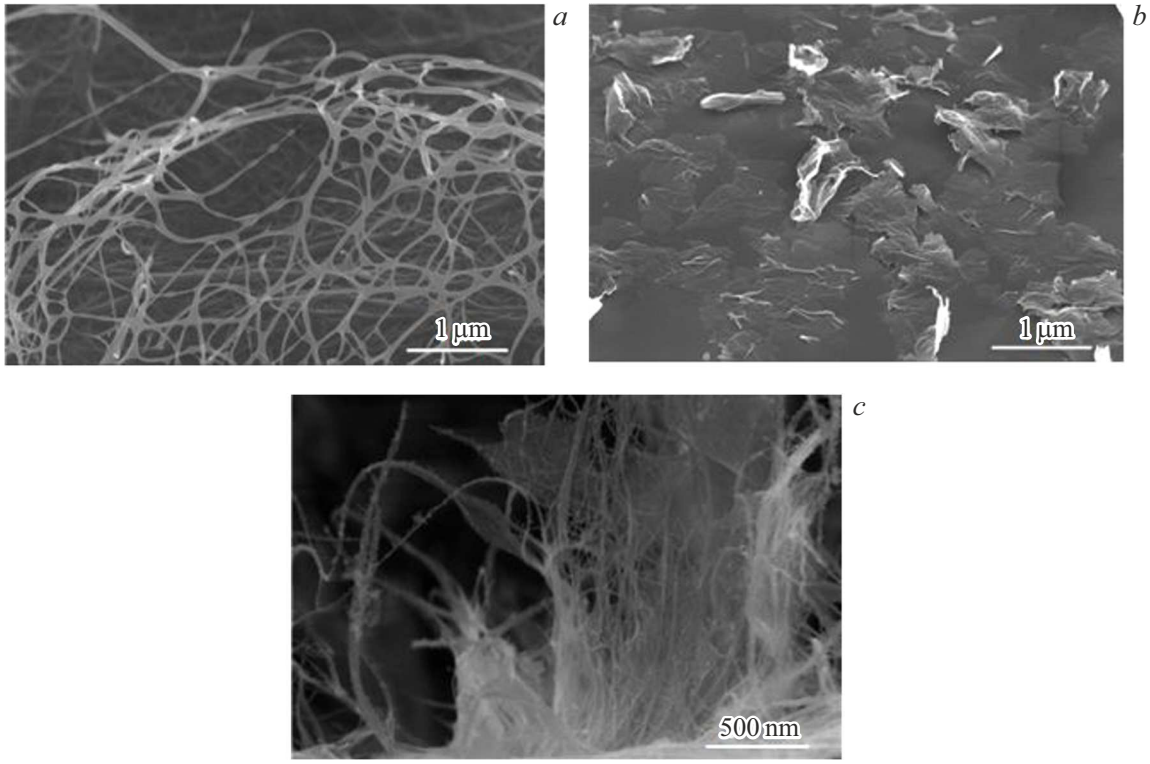


**Figure 5.** View of the samples: *a* — SWCNT, *b* — RGO, *c* — SWCNT and RGO hybrid structures exposed to 0.07 W laser radiation.

electrons with carbon nuclei [21] resulting in breaking the C−C bonds in the RGO structure. Chemical bonds are formed on the contact surface of the bonded SWCNT and RGO. This causes reconstruction of graphene layer surfaces. As a result, SWCNT and RGO connections are formed to provide bonding with formation of pairs of carbon atom heptagons and pentagons [22]. Figure 5 shows images of the SWCNT, RGO and SWCNT/RGO hybrid structures recorded after 0.07 W laser radiation exposure.

In case of SWCNT sample, interconnected carbon nanotube networks may be observed when the sample is exposed to low-power laser radiation. It is also possible to observe that each nanotube forms from 2 to 4 interconnections with other nanotubes. Moreover, the networks make it possible to build standing structures supported on lower sample layers. For the RGO sample, these images clearly show that RGO particles exposed to laser radiation have lighter surface areas. When the surface was examined at an angle, it was found that RGO particles with light areas were regions lifted above the substrate surface as a result of laser exposure, while the rest particles were pressed closer or soldered to the substrate surface. In the case of the SWCNT and RGO hybrid structure sample, it can be seen that standing complex treelike structures, that include interconnected SWCNT networks and form bridges with RGO particles, were formed. The height of standing structures was about 30 $\mu$m. It also can be seen that SWCNT bridge connections cover a significant part of the RGO particle surface. Moreover, it can be seen that RGO particles are lifted above the surface and rest on the SWCNT bridge supports.

As laser radiation power increased, destruction of samples could be observed and finally resulted in reduction of electric conductivity. Figure 6 shows images of the SWCNT, RGO and SWCNT/RGO hybrid structures recorded after 0.14 W laser radiation exposure.

Thus, in case of the SWCNT sample, it can be seen that, as the laser radiation power increases up to 0.14 W, some groups of free standing nanotubes and nanotubes grouped in harnesses form twisted structures. In addition, failure of nanotube network interconnections is observed in some areas. This phenomenon can be explained by high laser radiation power due to which a part of structure of nanotubes with few interconnections was damaged. In the case when the RGO samples are exposed to 0.14 W laser radiation, it can be seen that the number of light areas, i.e. of RGO particles lifted above the substrate surface, increased. However, at the same time it can be found that particles were partially damaged on edges and in the center as a result of high-power laser radiation. At the same time, formation of spherical particles welded with each other can be seen on the edges of RGO particles. These particles are presumably amorphous carbon. The SWCNT and RGO hybrid structure sample exposed to 0.14 W laser radiation

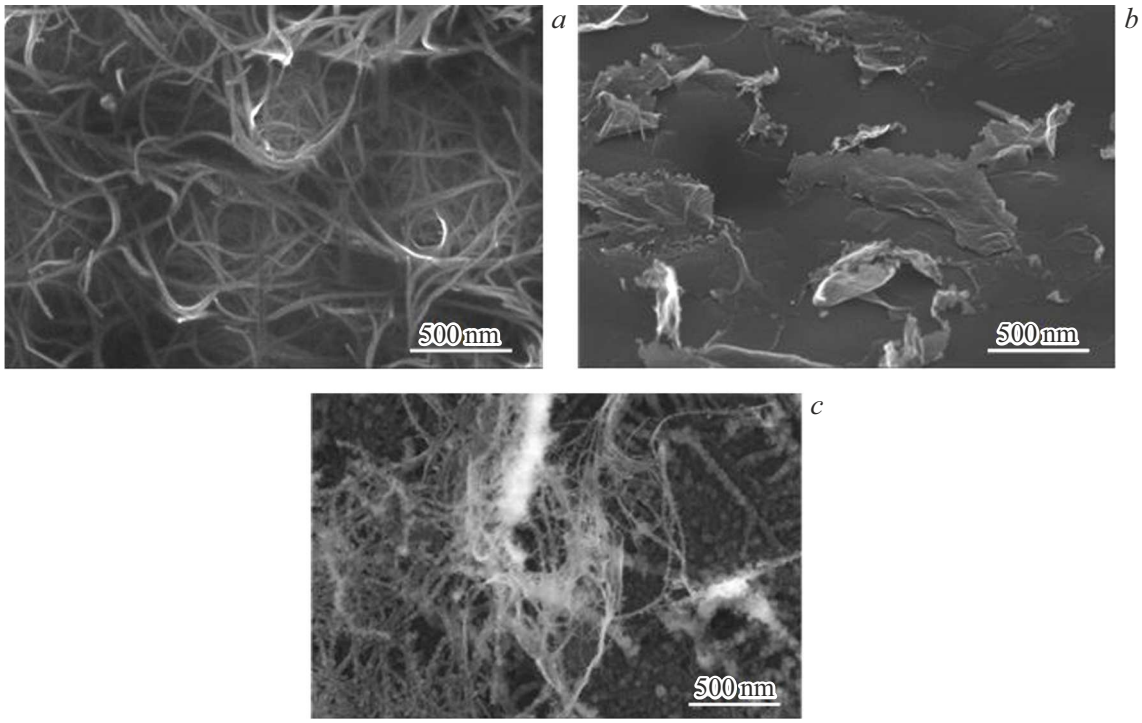


**Figure 6.** View of the samples: *a* — SWCNT, *b* — RGO, *c* — SWCNT and RGO hybrid structures exposed to 0.14 W laser radiation.

has a much less standing complex treelike structures and formation of amorphous carbon on their walls can be seen. These images show that lower layers of the coating were partially removed. As with the RGO sample, partial formation of amorphous carbon can be seen on the nanotube surfaces. At the same time, there were no areas where RGO particles were lifted using the SWCNT bridge supports.

Figure 7 shows images of the SWCNT, RGO and SWCNT/RGO hybrid compound recorded after 0.27 W laser radiation exposure.

When exposed to 0.27 W laser radiation, general visual inspection of the SWCNT sample surface shows significant failure of the external surface layer. Moreover, image magnification shows broken nanotube network interconnections and nanotube edges. These observations suggest that this laser power exceeds the threshold. When the RGO sample is exposed to 0.27 W laser radiation, much more light areas that are lifted above the substrate are observed, however, greater damage of RGO particles and formation of amorphous carbon is seen at the same time. When 0.27 W laser radiation is applied, images don't show any complex structures formed by the SWCNT and RGO hybrid compound. Few SWCNT interconnections with total absence of connections with RGO is observed. Significant amount of amorphous carbon formed by laser radiation on the nanotube surface was found . It can be seen that some lower layers of the sample were removed.

### 2.2. Raman scattering spectroscopy

Raman scattering spectroscopy assessed the effect of laser radiation on the formed SWCNT, RGO and SWCNT/RGO hybrid nanostructures (Figure 8). Several regions of interest can be highlighted on the recorded spectra: RBM vibrational mode ($100-400\,\mathrm{cm}^{-1}$) existing only on a carbon nanotube spectrum with the mode frequency inversely proportional to the nanotube diameter; band $D$ ($\sim 1350\,\mathrm{cm}^{-1}$) caused by defects and failures in the carbon lattice and band $G$ ($1580-1605\,\mathrm{cm}^{-1}$) that occurs in all carbon materials with $sp^2$-hybridization due to C−C bond strain in a hexagonal lattice. Intensity ratio of bands $D$ and $G$ is widely used as an indirect assessment of carbon material defect level, when the ratio increases, increase in the defect level and change in the structure of samples are observed.

In the case of samples based on SWCNT, as the density of laser radiation energy increased, gradual increase in the defect level was observed, typical mode frequencies shifted towards the values for amorphous carbon. Vibrational mode RBM remained at all laser radiation energies, which suggests that general structural features of SWCNT are retained and is supported by the SEM data.

Increase in the defect level with the increase in laser exposure power was also observed for the SWCNT and RGO hybrid compound. However, changes took place slower in this case, which may be explained by additional consumption of laser radiation energy for the change in graphene scale positions and formation of bonds between the sample components.

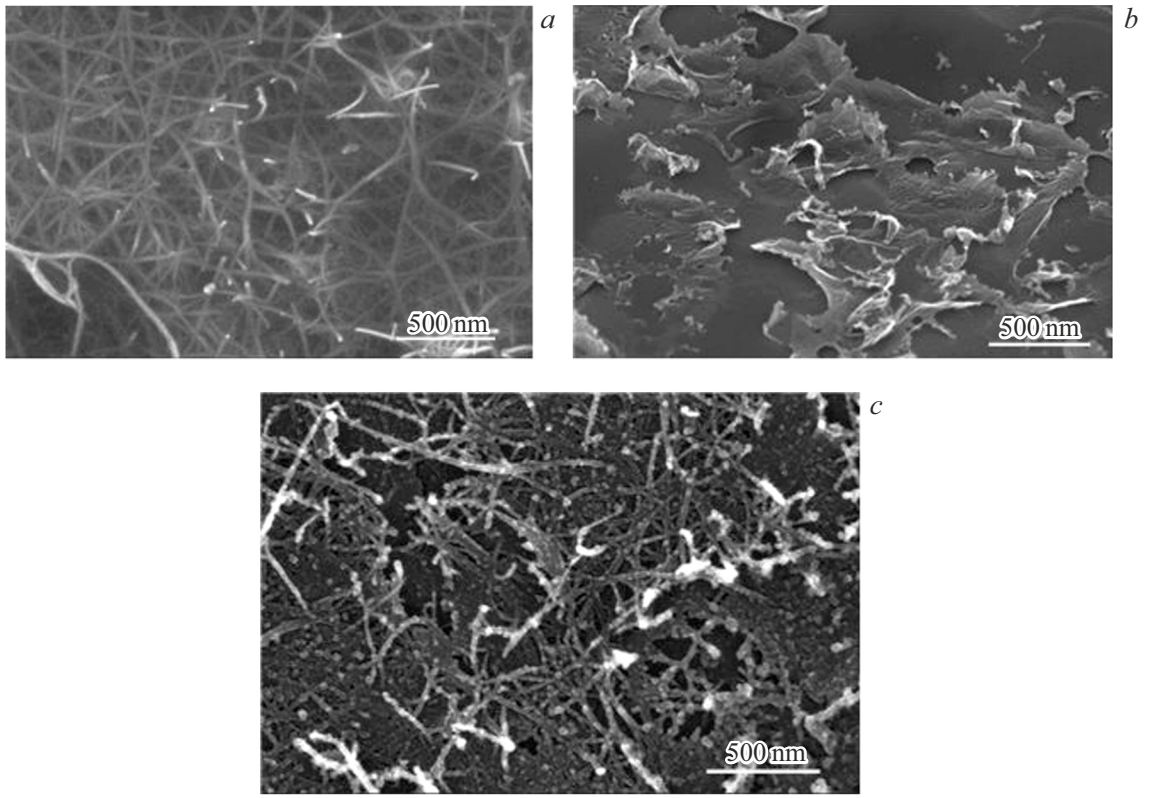


**Figure 7.** View of the samples: *a* — SWCNT, *b* — RGO, *c* — SWCNT and RGO hybrid compound exposed to 0.27 W laser radiation.

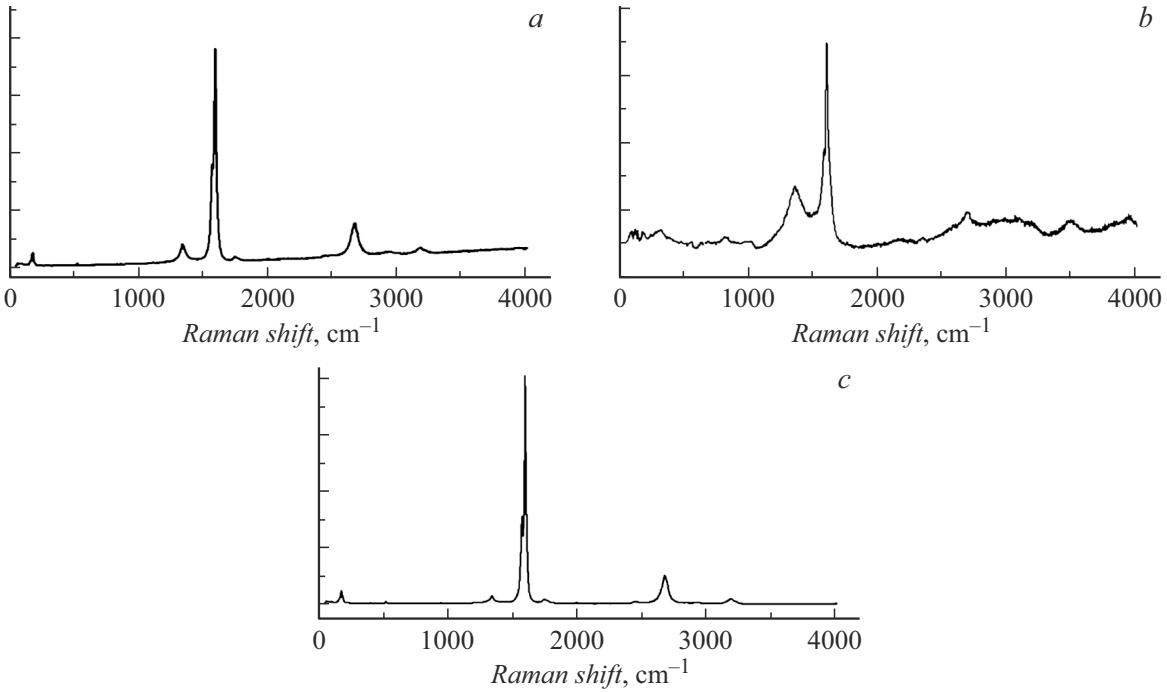


**Figure 8.** Raman scattering spectra of the samples: *a* — SWCNT, *b* — RGO, *c* — SWCNT and RGO hybrid compound.

Electric conductivities of samples and carbon scaffold nanomaterials in their original form and after laser irradiation with the specified power

| Samples | Laser radiation power, W | | | |
|---|---|---|---|---|
| | 0 | 0.07 | 0.14 | 0.27 |
| | Conductivity, mS | | | |
| SWCNT | $12.07 \pm 0.2$ | $30.0 \pm 0.8$ | $15.8 \pm 0.6$ | $11.6 \pm 0.6$ |
| RGO | $12.2 \pm 0.5$ | $15.4 \pm 0.2$ | $12.6 \pm 0.1$ | $12.3 \pm 0.2$ |
| SWCNT and RGO hybrid structures | $11.7 \pm 0.2$ | $37.8 \pm 1.2$ | $13.7 \pm 0.1$ | $11.8 \pm 0.3$ |

For the RGO samples, the intensity ratio of bands *D* and *G* gradually decreased as the laser radiation energy density increased. For this type of samples, analysis was hindered by the randomness of relative deposition of the graphene layers, and, consequently, the defect level covered all main typical modes. The rate of change of the defect level was much lower compared with that for pure nanotubes, while the width and intensity of bands *D* and *G* also decreased gradually. Welding of the graphene scales to the silicon substrate followed by graphene layer thinning probably took place.

### 2.3. Electric conductivity measurements

The table shows electric conductivity measurements of samples and carbon scaffold nanomaterials in their original form and after laser irradiation with the specified power.

It was found that change in the electric conductivity of samples takes place as the laser radiation power changes. At the same time, high electric conductivity is indicative of effective formation of the bonded SWCNT and RGO scaffold structure. When the SWCNT, RGO and SWCNT+RGO samples were exposed to 0.07 W laser radiation, their electric conductivities increased by a factor of 1.2 to 3.5 and were equal to $30.0 \pm 0.8$ mS, $15.4 \pm 0.2$ mS and $37.8 \pm 1.2$ mS, respectively. Increase in the laser radiation power resulted in electric conductivity reduction to values that were close to the initial one, therefore carbon scaffold nanomaterials for biotissue cell stimulation were formed at 0.07 W.

### 2.4. Cell growth on the topology surface

Fibroblast cell growth on the surfaces of samples in their original form and of carbon scaffold nanomaterials subjected to laser structuring was studied. Investigations were also conducted with and without electric cell growth stimulation. Electric stimulation is a well-known method used for cell control in various cell processes such as apoptosis, proliferation, differentiation and migration [23,24]. These processes take place due to the presence of cell transmembrane difference of potentials that is controlled by means of accumulation of ions with different concentrations inside and outside the cell. Concentrations of $Na^+$, $K^+$, $Ca^{2+}$, $Mg^{2+}$, $H^+$ and $Cl^-$ differ inside and outside the cell. Difference of potentials is controlled using ion channels and transporters. The concentration of $K^+$ prevails inside the cell, while the concentration of $Na^+$ prevails outside. Hodgkin and Huxley studies showed that, due to different concentration of $K^+$, energy occurred on the both sides of the membrane and generated voltage on the membrane. Due to nonuniform distribution of sodium ions, cell reaction is activated, and also due to sodium ions, activation of cell activity potential becomes possible. High concentration of sodium ions on the outside of the cell is balanced by the presence of negatively charged chlorine ions, and the concentration of potassium ions is balanced by the presence of negatively charged anions resulting in electrical neutrality inside and outside the cell.

Ion channels of the cell are responsible for charged particle transfer through the cell membrane. These channels may be both in closed and open states. Change in the states of channels generally occur due to changes in channel proteins and is defined by the factors arriving from the outside (exogenous signals) and inside (endogenous signals) the cell. In most cases, channel state is characterized randomly. However, there are signals that facilitate the change (increase or decrease) in the ion channel permeability and also the change in probability of detection of the protein structural configuration that facilitates state transition.

Potential at rest of most cells is characterized by a negative electric charge caused by high concentration of negative ions inside the cell compared with the concentration of negative ions outside the cell. Negative potential of rest causes the difference on potentials on the membrane that controls voltage-sensitive ion transfer and adenosine triphosphate (ATP) synthesis in mitochondria. Negative occurs partially due to the excess negative ions inside the cell (Donnan potential) and partially due to ionized groups on the membrane (surface potential). Electric stimulation changes the transmembrane potential of rest of the cell, which exerts a major effect on cell functionality and cell metabolism.

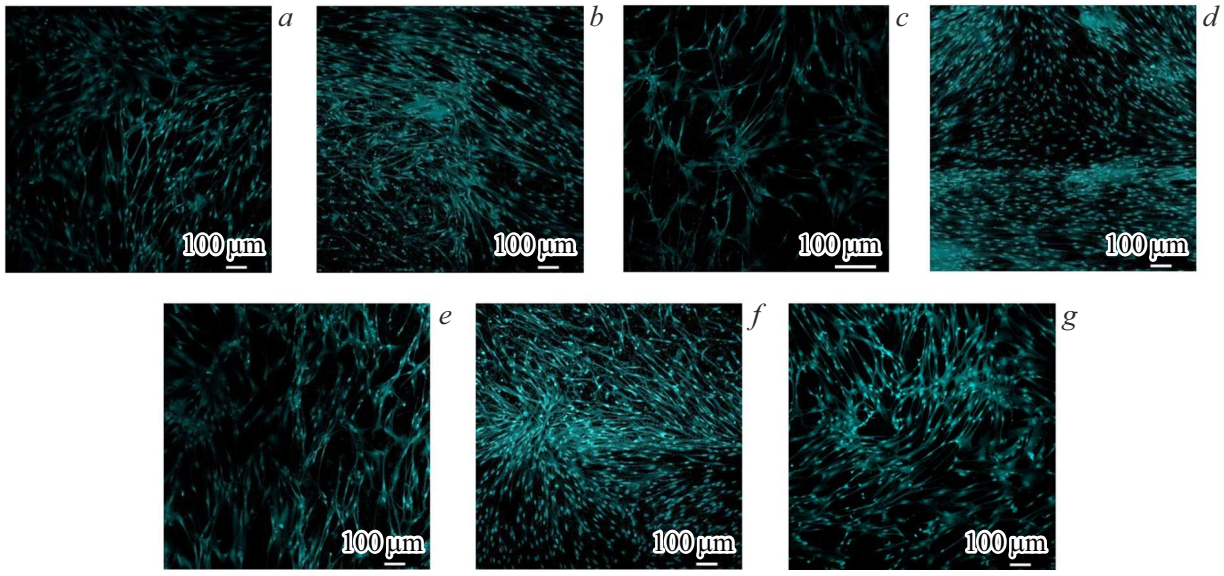


**Figure 9.** Images recorded after 72 h cultivation of FCL cells on carbon scaffold nanomaterial samples after laser structuring: *a, b* — SWCNT, *c, d* — RGO, *e,f* — SWCNT and RGO hybrid structures, *g* — control (pure silicon); *a, c, e, g* — without stimulation, *b, d, f* — with electric stimulation.

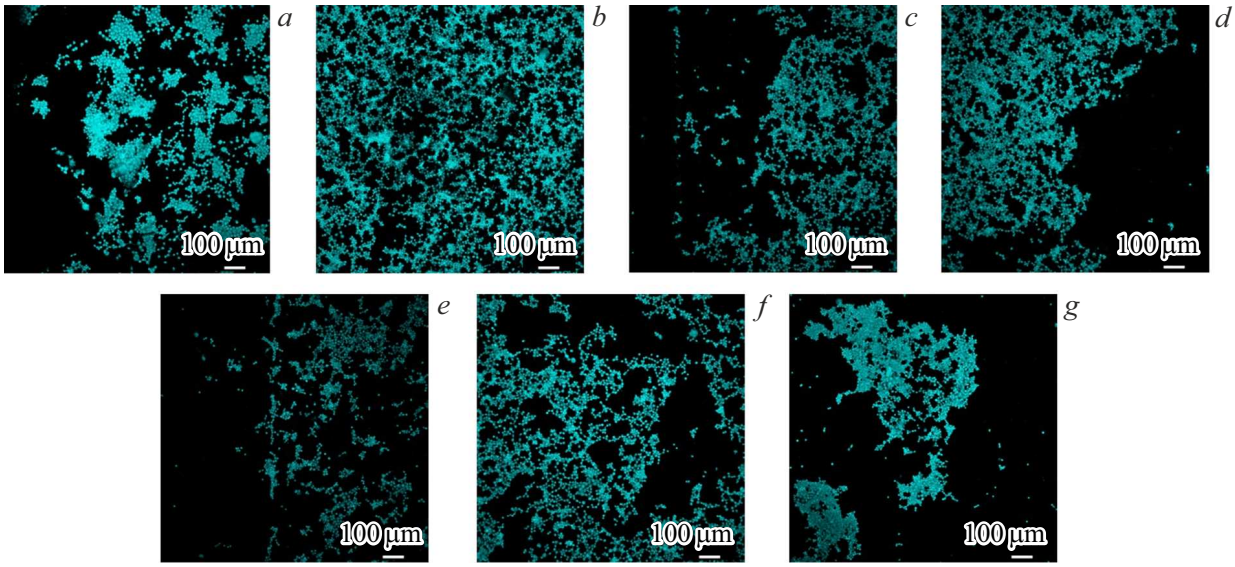


**Figure 10.** Images recorded after 72 h cultivation of Neuro 2A cells on carbon scaffold nanomaterial samples after laser structuring: *a, b* — SWCNT, *c, d* — RGO, *e,f* — SWCNT and RGO hybrid structures, *g* — control (pure silicon); *a, c, e, g* — without stimulation, *b, d, f* — with electric stimulation.

FCL cell microscopy on the sample surfaces are shown in Figure 9. The samples clearly show different areas of formed topologies. Cells on the carbon scaffold nanomaterial samples spread in width more actively compared with cells in nonconducting areas that have a thinner shape. Improved cell adhesion to nanomaterials is suggested. Cells in nanomaterial areas are primarily oriented in one direction. Cells on the carbon scaffold nanomaterial layers have a morphology similar to cell morphology on the controls, which means that the studied materials are not toxic.

microscopic images of Neuro 2A cells are shown in Figure 10. These cells don't form a monolayer and are more sensitive to cultivation conditions. Samples after electric stimulation clearly show that the carbon scaffold nanomaterial areas have more intense cell growth than the nonconducting parts of samples, which suggests that cell location can be controlled due to deposition of the required topology and electric stimulation. Electric stimulation makes it possible to achieve cell growth in smaller groups, which is favorable for their uniform distribution on the surface. The

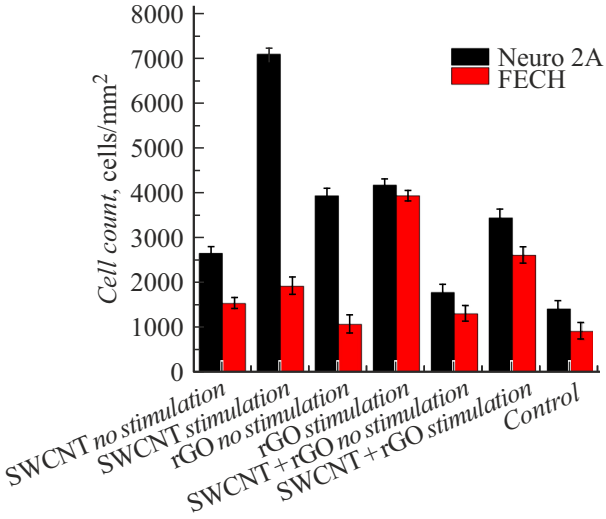


**Figure 11.** Number of cells on carbon scaffold nanomaterial samples for creating neurointerfaces compared with the control after 72 h of cultivation.

best growth of Neuro 2A cells was recorded on the SWCNT samples. The number of cells on the experimental samples exceeds this value for the control, while the regular cell morphology on the experimental samples is retained, which indicates that the studied samples are nontoxic.

The obtained data was used to count the cells in various topology areas for each of the samples. Graphical view of the results is shown in Figure 11. In this case, increase in the number of cells during electric stimulation by a factor of up to 2.6 was determined. The highest increase in the number of Neuro 2A cells during stimulation is observed for the SWCNT and SWCNT/RGO hybrid structure samples, which correlates with their higher electric conductivity compared with the RGO samples.

For connective tissue cells forming a monolayer during cultivation, the increase in the number of cells occurred during cultivation on samples based on reduced graphene oxide. It may be concluded that the scaly surface in this case makes a large contribution to cell growth due to improved cell adhesion to the RGO-based layer. The number of cells increased by a factor of 4.3 for FCL cells and by a factor of 2.9 for Neuro 2A cells compared with standard conditions on controls. The results suggest favorable effect of the fabricated nanomaterials on cell proliferation. Electric stimulation makes it possible to increase the number of various types of cells and to orient them in the desired direction. Cumulative impact of the electrically conductive scaffold and electric stimulation show higher results for electrically conductive cells, however, more active proliferation for connective tissue cells is associated not only with electric conductivity, but also with more suitable surface structure that is favorable for cell adhesion. These nanomaterials may find application in fields of electric pulse transport in implanted neurointerfaces, and nanomaterial processing techniques may be used to create materials for microelectronic applications and feedback systems for pain syndrome diagnosis and treatment.

## Conclusion

The work describes the results of study of carbon scaffold nanomaterials used as interfaces for stimulation of conductive and nervous tissue cells. A technique is proposed to form desired topologies from scaffold nanomaterials by spray deposition of SWCNT, RGO, SWCNT/RGO hybrid structure layers followed by structuring and sublimation under laser radiation with different power. It was found that carbon scaffold nanomaterials after $\geq .07$ W laser structuring are characterized by formation of bonds between SWCNT and RGO and branched structure due to photon-phonon interaction. Lifted complex treelike RGO structures, including interconnected SWCNT networks that form bridge connections with RGO scales, were formed. Such scaffold nanomaterials have higher electric conductivity, this effect is exhibited particularly well or samples consisting of SWCNT/RGO hybrid structures. When using 0.07 W laser radiation structuring, electric conductivities for the SWCNT, RGO and SWCNT+RGO samples increased by a factor of 1.2 to 3.5 and were equal to $30.0 \pm 0.8$ mS, $15.4 \pm 0.2$ mS and $37.8 \pm 1.2$ mS, respectively. Electric conductivity of scaffold nanomaterials not lower than the values for connective and nervous tissues is one of the key requirements for interfaces for stimulating devices. Positive effect of the influence of carbon scaffold nanomaterials on cell growth was demonstrated. Electric stimulation during cultivation ensures an increase in the number of cells. The number of cells increased by a factor of 4.3 for FCL cells and by a factor of 2.9 for Neuro 2A cells compared with standard conditions. Thus, investigations of the formed scaffold nanomaterials demonstrate that these materials are promising for application as neurointerfaces for effective transmission of electric signals, cell cultivation devices and other implantable devices.

### Funding

This study was performed as part of a large research project and funded by the Russian Federation represented by the Ministry of Science and Higher Education of the Russian Federation under Agreement № 075-15-2024-555 dated October 25, 2024.

### Conflict of interest

The authors declare no conflict of interest.

## References

[1] S.H. Ku, M. Lee, C.B. Park. Adv. Healthcare Mater., **2** (2), 244 (2013). https://doi.org/10.1002/adhm.201200307

[2] C. Satishkumar, P.J. Thomas, A. Govindaraj, C.N.R. Rao. Appl. Phys. Lett., **77**, 2530 (2000). https://doi.org/10.1063/1.1319185
[3] M. Terrones, F. Banhart, N. Grobert, J.C. Charlier, H. Terrones, P.M. Ajayan. Phys. Rev. Lett., **89**, 075505 (2002). https://doi.org/10.1103/PhysRevLett.89.075505
[4] J. Kim, G.G. Kim, S. Kim, W. Jung. Appl. Phys. Lett., **108**, 203110 (2016). https://doi.org/10.1063/1.4952397
[5] G. Ho, A. Wee, J. Lin. Appl. Phys. Lett., **79**, 260 (2001). https://doi.org/10.1063/1.1383279
[6] J. Han, M.P. Anantram, R.L. Jaffe, J. Kong, H. Dai. Phys. Rev. B, **57** (23), 14983 (1998). https://doi.org/10.1103/PhysRevB.57.14983
[7] M. David-Pur, L. Bareket-Keren, G. Beit-Yaakov, D. Raz-Prag, Y. Hanein. Biomed. Microdevices, **16**, 43 (2014). DOI: 10.1007/s10544-013-9804-6
[8] B.C. Kang, T.J. Ha. Jpn. J. Appl. Phys., **57** (5S), 05GD02 (2018). DOI: 10.7567/JJAP.57.05GD02
[9] Y. Qiao, X. Li, T. Hirtz, G. Deng, Y. Wei, M. Li, S. Ji, Q. Wu, J. Jian, F. Wu, Y. Shen, H. Tian, Y. Yang, T.L. Ren. Nanoscale, **11** (41), 18923 (2019). DOI: 10.1039/C9NR05532K
[10] Q.L. Zhao, Z.M. Wang, J.H. Chen, S.Q. Liu, Y.K. Wang, M.Y. Zhang, J.-J. Di, G.-P. He, L. Zhao, T.-T. Su, J. Zhang, X. Liang, W.-L. Song, Z.L. Hou. Nanoscale, **13** (24), 10798 (2021). DOI: 10.1039/D0NR08032B
[11] A. Kuksin, D. Murashko, A. Gerasimenko. *Ural-Siberian Conference on Computational Technologies in Cognitive Science, Genomics and Biomedicine* (CSGB), IEEE, 250 (2022). DOI: 10.1109/CSGB56354.2022.9865613
[12] N. Nekrasov, N. Yakunina, V. Nevolin, I. Bobrinetskiy, P. Vasilevsky, A.Y. Gerasimenko. Biomimetics, **6** (4), 66 (2021). DOI: 10.3390/biomimetics6040066
[13] A.Y. Gerasimenko, A.V. Kuksin, Y.P. Shaman, E.P. Kitsyuk, Y.O. Fedorova, D.T. Murashko, A.A. Shamanaev, E.M. Eganova, A.V. Sysa, M.S. Savelyev, D.V. Telyshev, A.A. Pavlov, O.E. Glukhova. Nanomaterials, **12** (16), 2812 (2022). DOI: 10.3390/nano12162812
[14] A.Yu. Gerasimenko, E. Kitsyuk, U.E. Kurilova, I.A. Suetina, L. Russu, M.V. Mezentseva, A. Markov, A.N. Narovlyansky, S. Kravchenko, S.V. Selishchev, O.E. Glukhova. Polymers, **14** (9), 1866 (2022). DOI: 10.3390/polym14091866
[15] A.Y. Gerasimenko, A.V. Kuksin, Y.P. Shaman, E.P. Kitsyuk, Y.O. Fedorova, A.V. Sysa, A.A. Pavlov, O.E. Glukhova. Nanomaterials, **11**, 1875 (2021). DOI: 10.3390/NANO11081875
[16] A.Y. Gerasimenko, G.N. Ten, D.I. Ryabkin, N.E. Shcherbakova, E.A. Morozova, L.P. Ichkitidze. Spectrochim. Acta Part A Mol. Biomol. Spectrosc., **227**, 117682 (2020). DOI: 10.1016/j.saa.2019.117682
[17] M.S. Savelyev, A.Y. Gerasimenko, P.N. Vasilevsky, Y.O. Fedorova, T. Groth, G.N. Ten, D.V. Telyshev. Anal. Biochem., **598**, 113710 (2020). DOI: 10.1016/J.AB.2020.113710
[18] A.Y. Gerasimenko, U.E. Kurilova, M.S. Savelyev, D.T. Murashko, O.E. Glukhova. Compos. Struct., **260**, 113517 (2021). DOI: 10.1016/j.compstruct.2020.113517
[19] A.Y. Gerasimenko, U.E. Kurilova, I.A. Suetina, M.V. Mezentseva, A.V. Zubko, M.I. Sekacheva, O.E. Glukhova. Appl. Sci., **11**, 8036 (2021). DOI: 10.3390/APP11178036
[20] N.A. Demidenko, A.V. Kuksin, V.V. Molodykh, E.S. Pyankov, L.P. Ichkitidze, V.A. Zaborova, A.A. Tsymbal, S.A. Tkachenko, H. Shafaei, E. Diachkova, A.Yu. Gerasimenko. Bioeng., **9**, 36 (2022). DOI: 10.3390/BIOENGINEERING9010036
[21] Y. Yuan, J. Chen. Laser Phys. Lett., **13** (2016). DOI: 10.1088/1612-2011/13/6/066001
[22] L. Chico, V.H. Crespi, L.X. Benedict, S.G. Louie, M.L. Cohen. Phys. Rev. Lett., **76**, 971 (1996). DOI: 10.1103/PHYSREVLETT.76.971
[23] M. Griffin, S.A. Iqbal, A. Sebastian, J. Colthurst, A. Bayat. PLoS One, **6**, e23404 (2011). DOI: 10.1371/journal.pone.0023404
[24] N. Matsuki, M. Takeda, T. Ishikawa, A. Kinjo, T. Hayasaka, Y. Imai, T. Yamaguchi. Oncol. Rep., **23**, 1425 (2010). DOI: 10.3892/OR_00000780/HTML

*Translated by E.Ilinskaya*